Supplementary: Dynamical decoherence of the light induced interlayer coupling in $YBa_2Cu_3O_{6+\delta}$

C. R. Hunt[1,4], D. Nicoletti[1], S. Kaiser[1,3], D. Proepper[3], T. Loew[3], J. Porras[3], B. Keimer[3], A. Cavalleri[1,2]

[1] *Max Planck Institute for the Structure and Dynamics of Matter, Hamburg, Germany*

[2] *Department of Physics, Oxford University, Clarendon Laboratory, Oxford, United Kingdom*

[3] *Max Planck Institute for Solid State Research, Stuttgart, Germany*

[4] *Department of Physics, University of California Berkeley, Berkeley, California, USA*

S1. Calculation of the transient complex optical response

The experiment was performed in reflection geometry, with the pump beam striking the sample at normal incidence and the THz probe p-polarized at 30°. The reflected probe field in the absence of excitation, $E(t)$, and the pump-induced changes to the field at each time delay τ, $\Delta E(t,\tau)$, were measured via electro-optic sampling and then independently Fourier transformed to extract the changes in the complex reflection coefficient $\tilde{r}'$, $\Delta\tilde{E}(\omega,\tau)/\tilde{E}(\omega) \equiv (\tilde{r}' - \tilde{r}_0)/\tilde{r}_0$. The equilibrium $\tilde{r}_0$ was taken from a separate measurement (see section S2).

The THz field samples a crystal volume up to ~20 times greater than the mid-infrared pump (Figure S1.1.B). In order to isolate the THz response of the excited region alone, the system was modeled as a single excited layer, with complex refractive index $\tilde{n}(\omega)$, on top of a region that remains in equilibrium, with refractive index $\tilde{n}_0(\omega)$.[1] The excited layer thickness was set to the pump penetration depth d_p. A cartoon of this configuration is shown in Figure S1.1.C as a light purple excited layer on top of the equilibrium bulk in grey.

For comparison, we also utilized a multilayer approach, which treats the surface as a stack of m thin layers, Δz, with refractive index decaying to its bulk value, $\tilde{n}(\omega) = \tilde{n}_0(\omega) + \Delta\tilde{n}(\omega)e^{-m\Delta z/d_p}$ (see also Ref. 2 and 3). This is depicted in the cartoon as the dark purple region. Both methods produced virtually identical results, as shown in Figure S1.2 for YBCO 6.5 at 100 K.

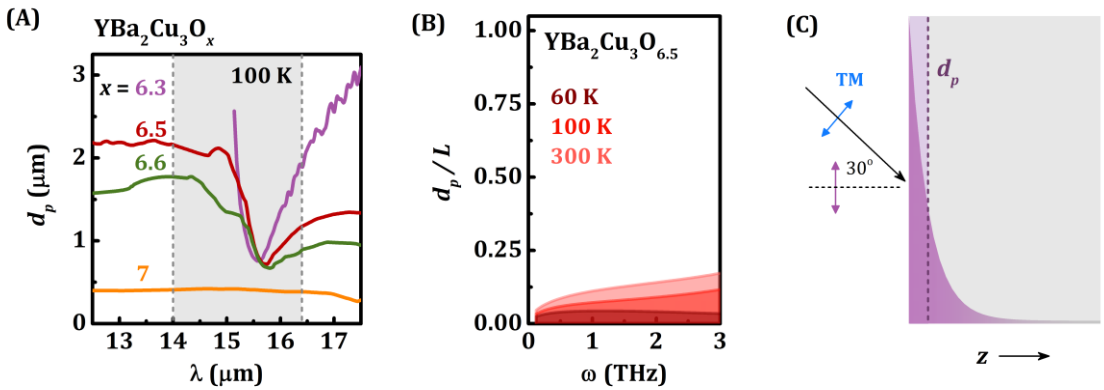

Figure S1.1: Modeling the photo-excited crystal. (A) Frequency-dependent penetration depth of YBCO in the spectral region of the apical oxygen phonon. Dashed lines indicate the FWHM of the pump spectrum. Note that, due to the absence of electronic screening in all underdoped samples, d_p shows no doping dependence at the phonon peak frequency for $x \leq 6.6$. **(B)** Pump-probe penetration depth mismatch for YBCO 6.5 at different temperatures. The pump penetration depth d_p is taken at the minimum value at the phonon resonance. The frequency-dependent THz probe penetration depth is labeled L. **(C)** A cartoon depicting the excited sample and the pump-probe geometry. The pump impinges on the sample at normal incidence and excites a region at the sample surface. The photo-excited crystal is modeled as a single excited layer of thickness d_p on an unperturbed bulk. This model agrees well with a second model that treats the excited layer as having a refractive index $\tilde{n}(\omega)$ at the surface that decays exponentially with depth z to the equilibrium value $\tilde{n}_0(\omega)$.

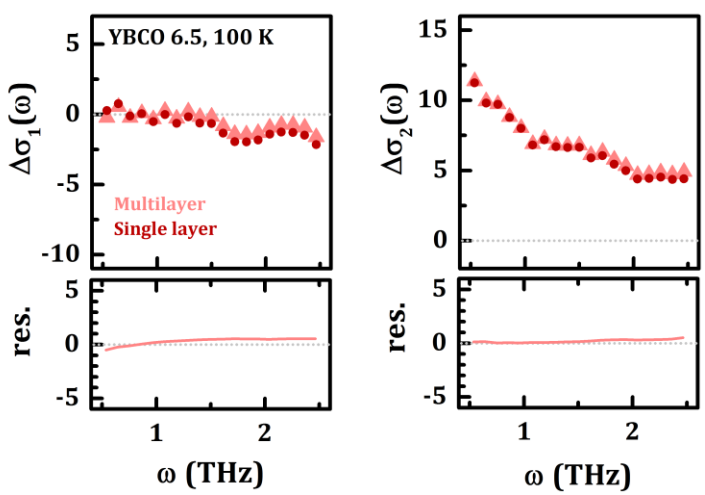

Figure S1.2: Comparison of multilayer and single layer models. The light-induced changes to the complex conductivity for YBCO 6.5 at 100 K, at $\tau = 0.8$ ps after excitation. The residual difference between the models is shown below the conductivity.

S2. Equilibrium optical response of $YBa_2Cu_3O_{6.3}$

Since the c-axis optical response of YBCO at $T > T_c$ is flat and featureless in the 0.5-2.5 THz region, normalization of the transient spectra could be performed using literature data.[4,5,6] In addition, the c-axis equilibrium broadband dielectric function of YBCO 6.3 was measured on the same sample used for the pump-probe experiment, using far-infrared ellipsometry. These were then extended to $\omega \to 0$ using Drude-Lorentz fits (see Fig. S2.1). $\sigma_1(\omega \to 0)$ follows the high temperature dc resistivity trend, $\rho_0 \propto 1/T$, and the exponential doping dependence found in literature[7] (see Figure S2.2).

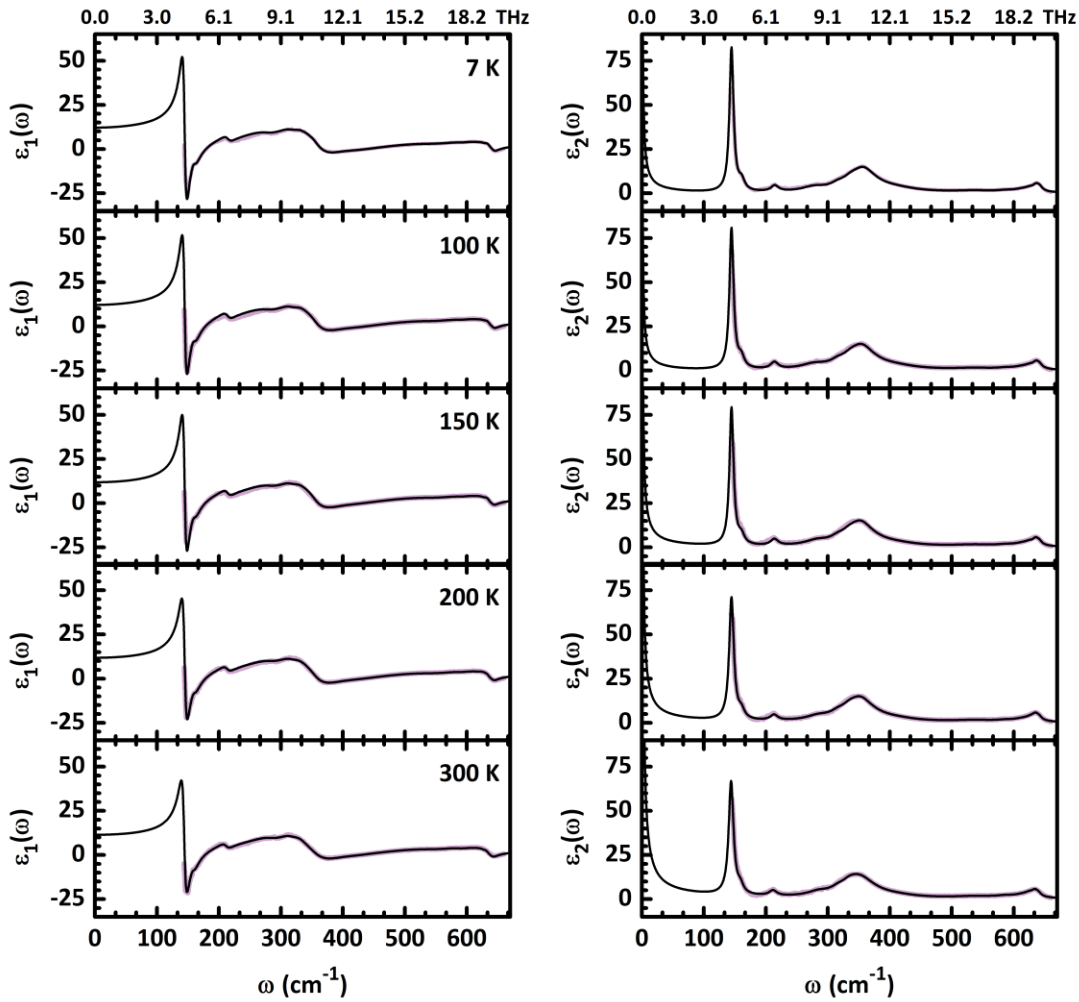

Figure S2.1: Complex dielectric function of $YBa_2Cu_3O_{6.3}$. Experimental data in purple, Drude-Lorentz fit in black.

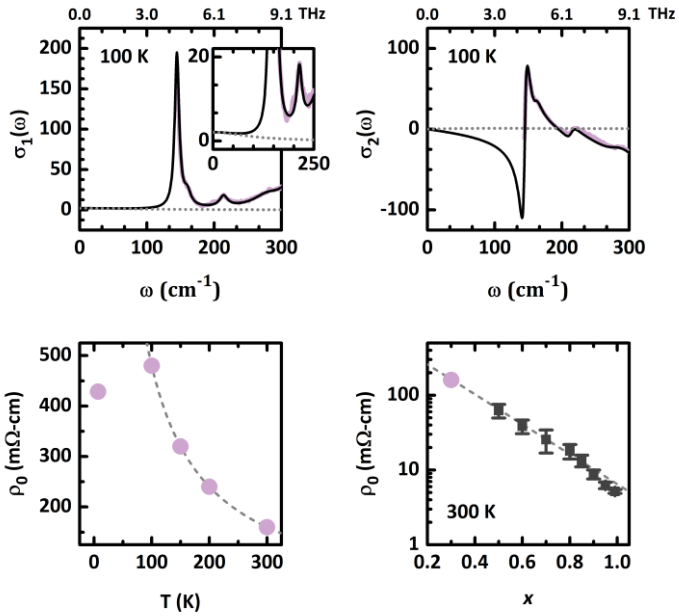

Figure S2.2: Temperature and doping trends in the quasi dc conductivity. Top row: The low frequency conductivity (in units $1/\Omega$-cm) calculated from the complex dielectric function, using $\varepsilon_\infty = 4.7$ (purple). Drude-Lorentz fits are shown in black. The Drude component is also plotted separately (dotted grey line). **Bottom row, left panel:** The estimated dc resistivity, $\rho_0 = 1/\sigma_1(\omega \to 0)$, following the trend $\rho_0 \propto 1/T$ for $T > 100$ K, as seen in literature for lower doped compounds. **Right panel:** Linear scaling of resistivity with doping. Black squares are data from Ref. 7.

S3. The light-induced response in YBCO 6.3

Here in Fig. S3.1 we report the full complex conductivity of YBCO 6.3 at the peak of the response ($\tau =$ 0.8 ps), at several temperatures (similar plots for YBCO 6.45-6.6 have already been reported in Ref. 2.) Black dashed lines indicate effective medium fits, as discussed in the main text.

Around 200 K, the best-fit photo-susceptible volume fraction f approaches the percolation threshold, which is $f \geq 33\%$ for the Bruggeman form in Equation 2 in the main text (assuming spherical inclusions for the sake of simplicity). This response can also be fit with a single plasma mode, Eq. 1 in the main text, describing a material with metallic or superconducting inclusions with a volume fraction f beyond the percolation threshold. Figure S3.2 shows a comparison between a single medium and an effective medium fit to the response at 200 K. Note that the small response in our THz frequency window, which cuts off above the plasma frequency, makes distinguishing these regimes difficult.

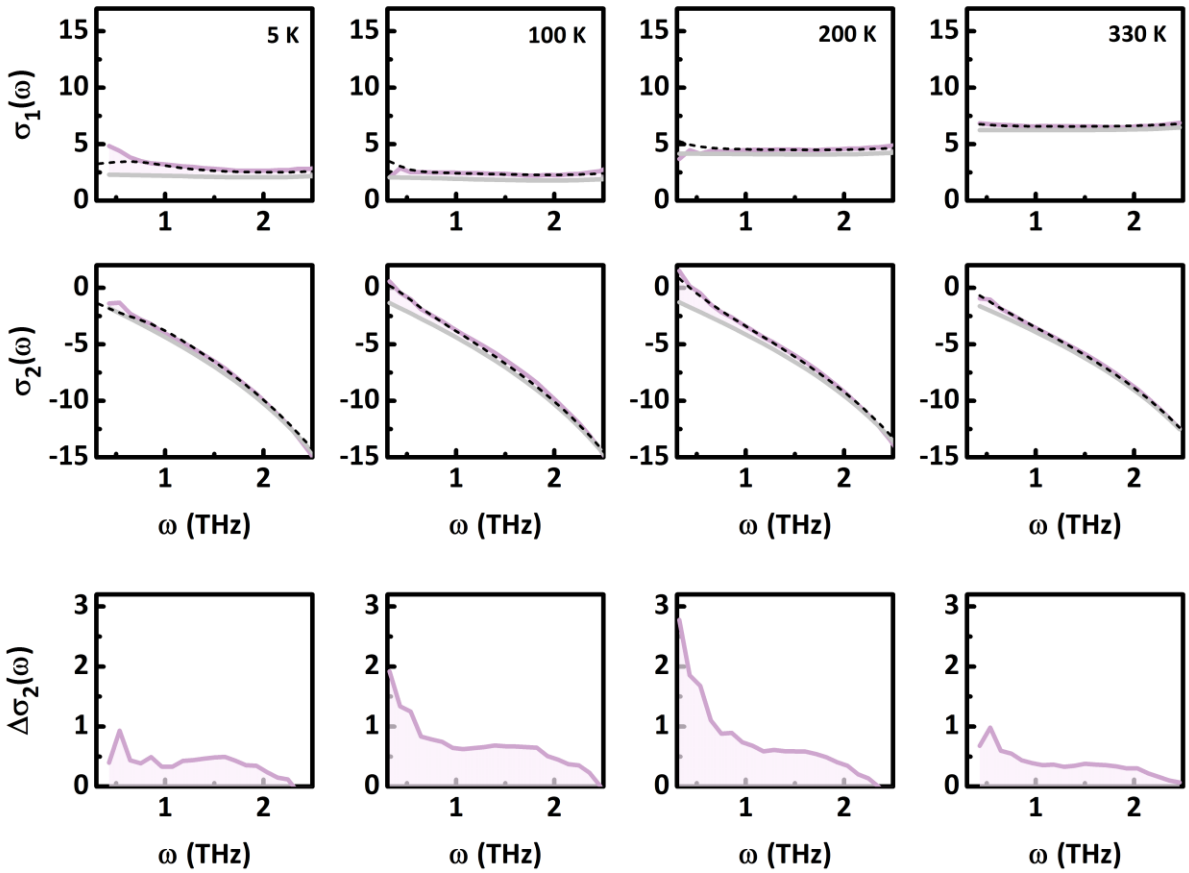

Figure S3.1 Complex conductivity of photo-excited YBCO 6.3 at 5 K, 100 K, 200 K, and 330 K. Real (top row) and imaginary (middle row) conductivity at $\tau = 0.8$ ps after excitation is shown in purple in units $1/\Omega$-cm. Effective medium fits appear as black dashed lines. Equilibrium conductivity is in grey. The light induced changes to the inductive conductivity, $\Delta\sigma_2(\omega) = \sigma_2(\omega, \tau = 0.8\text{ ps}) - \sigma_{2,eq}(\omega)$, (bottom row) show a $1/\omega$-like increase to low frequency.

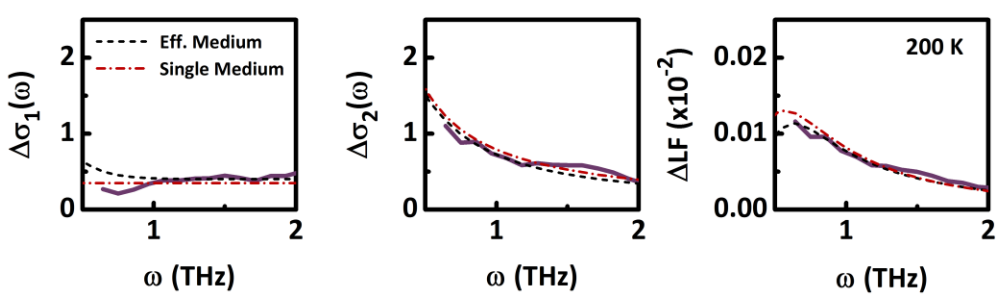

Figure S3.2 Comparison of effective medium and single plasmon fits to YBCO 6.3 at 200 K. Light-induced changes in the real (left) and imaginary (middle) conductivity and the loss function (right). Measured response is shown in purple, the single plasmon fits with black dashed lines, and the effective medium fit with grey dotted lines. The effective medium fit uses a photo-excited volume of $f = 32\%$.

S4. Effect of pumping an in-plane phonon mode

An in-plane phonon mode of B_{3u} symmetry also falls near 15 μm (see Fig. 3A). This is a Cu-O stretching mode in CuO_2 plane; analogous to the phonon resonantly excited in the experiments on lanthanides.[8] The planar lattice motions due to this mode are illustrated in Fig. S4B. Fig. S4C-D plots the changes in the real and imaginary conductivity of YBCO 6.5 at 300 K after excitation with 15-μm pulses polarized along the *a*-axis (B_{3u} mode pumping) and *c*-axis (B_{1u} mode pumping). No enhanced inductive response is observed after *a*-axis pumping; instead $\sigma_2(\omega)$ reduces. This result further highlights the importance of the apical oxygen mode excitation.

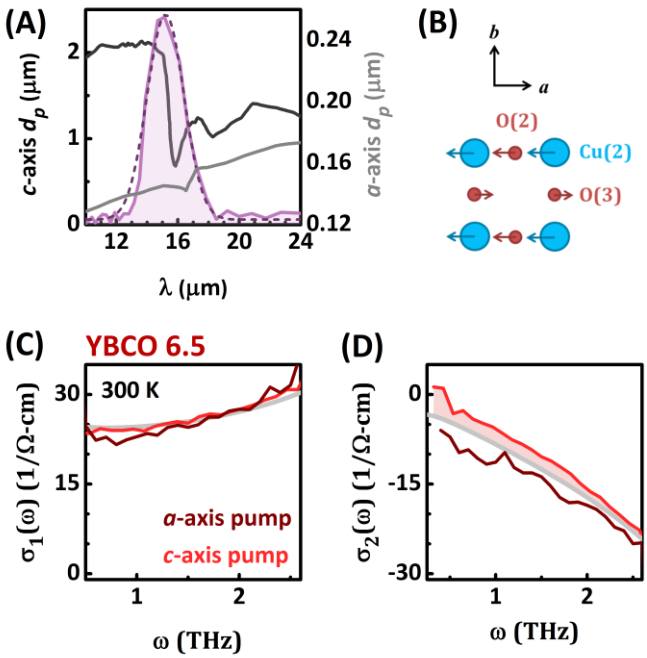

Figure S4. Excitation of a B_{3u} in-plane Cu-O stretching mode in YBCO 6.5. (A) The pump penetration depth d_p along the *c*-axis (black) and *a*-axis (grey). The kink in each profile indicates the frequency of the B_{1u} and B_{3u} phonon modes respectively. The pump spectrum is overlayed atop (purple) with a Gaussian fit (dashed line). The spectrum width is 1.5 μm. **(B)** A cartoon of the Cu (blue) and O (red) atoms in the CuO_2 planes. Arrows indicate the motion of the B_{3u} mode. The bottom row plots the pump-induced changes to the **(C)** real and **(D)** imaginary conductivity probed along the *c*-axis. Both *c*-axis (red) and *a*-axis (dark red) pumping induce little change in $\sigma_1(\omega)$. The $\sigma_2(\omega)$ response is quite different, however, with only B_{1u} (*c*-axis) mode excitation producing a positive change.

S5. The time evolution of the inductive response

The relaxation of the light-induced plasma mode appears governed by a loss of coherence, which can be seen in terms of a suppression of the low frequency $\omega\Delta\sigma_2(\omega)$, which deviates from a constant behavior. Here we report an extensive analysis of the relaxation performed on YBCO 6.45, where the inductive response is large and the quasiparticle component is minimal at all temperatures.

Figure S5.1 shows $\omega\Delta\sigma_2(\omega)$ at different time delays, for several temperatures between 45 K and 300 K ($T_c = 35$ K). All data feature the same behavior. A flat $\omega\Delta\sigma_2(\omega)$ at early delays gives way first to a drop in the low frequency response below a frequency ω^*. The downturn point ω^* shifts to higher frequency with time and is joined with an overall depression of the $\omega\Delta\sigma_2(\omega)$ level above ω^*. The frequency-averaged $\langle\omega\Delta\sigma_2(\omega)\rangle$ above ω^* was extracted as a function of time at all temperatures and is plotted in Figure S5.2. The error bars reflect the standard deviation of $\langle\omega\Delta\sigma_2(\omega)\rangle$. The decay was fit with a double exponential to extract the timescales of the relaxation plotted in Fig. 4 of the main text.

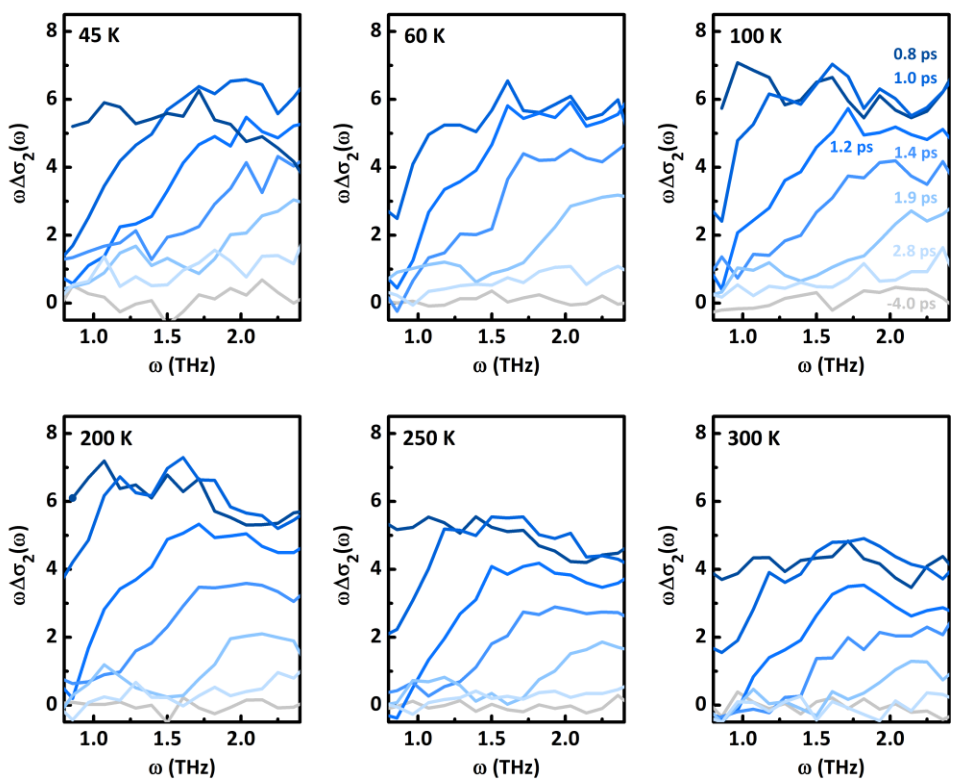

Figure S5.1: The inductive response $\omega\Delta\sigma_2(\omega)$ for YBCO 6.45 at several temperatures between 45 K and 300 K. Time delays are shown between 0.8 ps and 2.8 ps, with color code in the top-right panel.

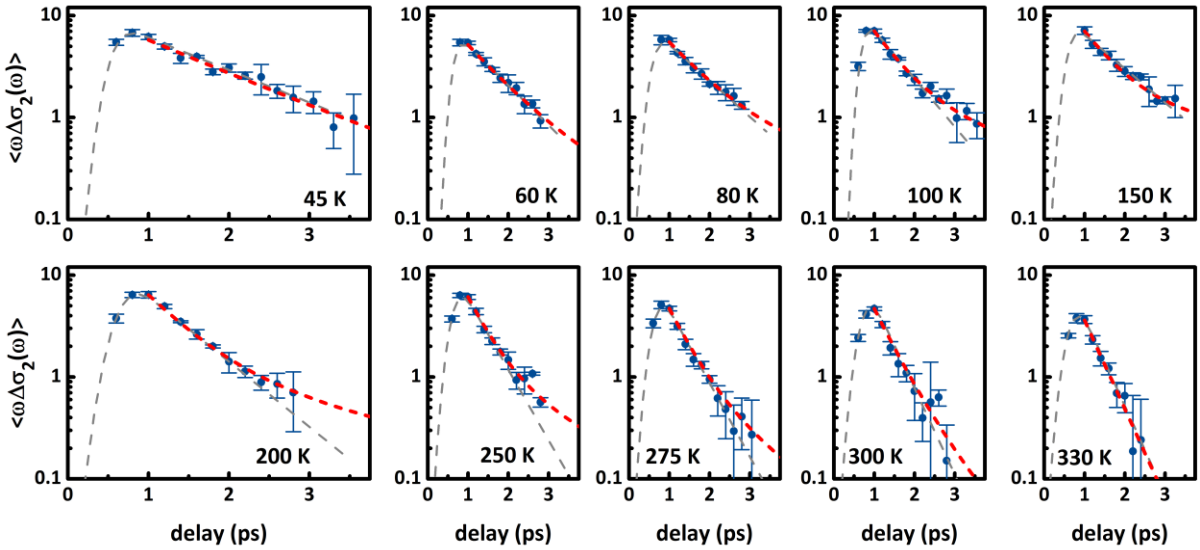

Figure S5.2: The relaxation timescales of $\langle \omega \Delta \sigma_2(\omega) \rangle$. The mean $\langle \omega \Delta \sigma_2(\omega) \rangle$, averaged where the response remains flat, is shown as a function of time for temperatures between 45 K and 330 K. The grey dashed lines indicate fits to a single exponential, plus error function to capture the behavior around the peak of the response. The red dashed lines are double exponential fits which more accurately capture the relaxation on longer time scales. The weight of each exponential component was held constant, with $\omega \Delta \sigma_2(\omega) \propto 0.8 e^{-t/\tau_1} + 0.2 e^{-t/\tau_2}$.

S6. The splitting of the light-induced plasma mode

Fits to the optical conductivity attribute the drop in $\langle \omega \Delta \sigma_2(\omega) \rangle$ to a decrease in the volume fraction f rather than a drop in the plasma frequency ω_p. Figure S6.1A shows effective medium fits to the loss function of the light-induced state at a few time delays. From these fits, the plasma mode contribution, $\mathrm{Im}(-1/\tilde{\varepsilon}_a)$, is extracted and plotted in Figure S6.1B, where $\tilde{\varepsilon}_a = \tilde{\varepsilon}_p$ at early time delays (see Eq. 1, main text) and $\tilde{\varepsilon}_a = \tilde{\varepsilon}_{2p}$ at later time delays (see Eq. 3, main text). The plasma frequency $\omega_p' = \omega_p/\sqrt{\varepsilon_\infty}$ is plotted as a function of time in panel S6.1C, showing the splitting of the plasmon at later delays. The filling fraction f (Fig. S6.1D) relaxes with time following the double exponential behavior similar to that seen in $\langle \omega \Delta \sigma_2(\omega) \rangle$.

The splitting of the light-induced plasma mode is seen at all dopings and across all temperatures measured. Figure S6.2 shows the plasma mode for all four underdoped compounds, presented as a peak in the loss function $\Delta LF = \mathrm{Im}(-1/\tilde{\varepsilon}\,) - \mathrm{Im}(-1/\tilde{\varepsilon}_{eq})$, at two time delays after excitation. At 1 ps, the single peak in the response corresponds to a single plasma mode. By 1.8 ps after excitation, the peak has split into two peaks separated by ~1 THz, indicating two plasma modes.

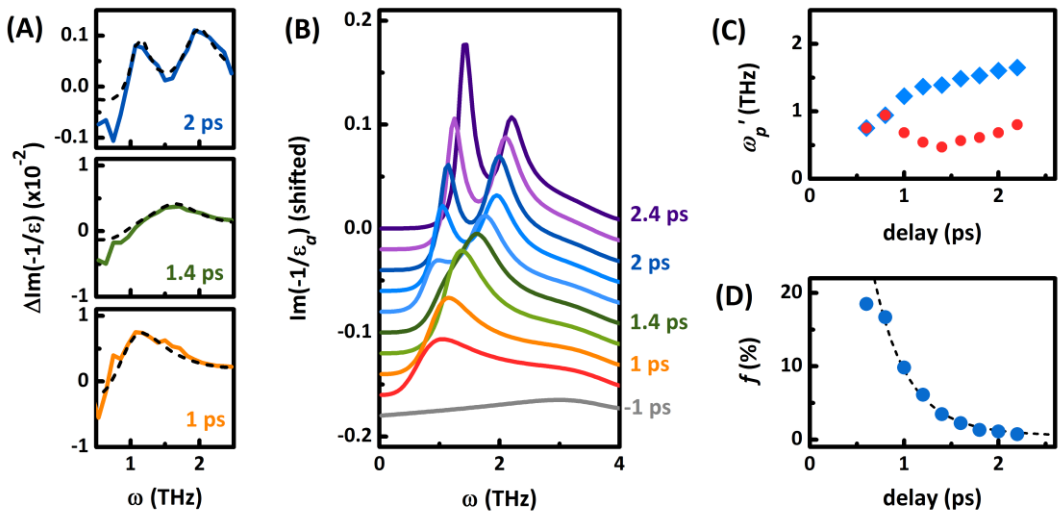

Figure S6.1: Time evolution of the light-induced plasma mode in YBCO 6.45 at 200 K. (A) The light-induced changes to the loss function $\Delta\mathrm{Im}(-1/\tilde{\varepsilon}\,) = \mathrm{Im}(-1/\tilde{\varepsilon}\,) - \mathrm{Im}(-1/\tilde{\varepsilon}_{eq})$ at three time delays after excitation. Dashed lines are effective medium fits. **(B)** The loss function $\mathrm{Im}(-1/\tilde{\varepsilon}_a)$ of a single plasma mode ($\tau \lesssim 1.0$ ps) or split plasma mode ($\tau \gtrsim 1.0$ ps) used in the fits ($\tilde{\varepsilon}_a = \tilde{\varepsilon}_p$ in Eq. 1 and $\tilde{\varepsilon}_a = \tilde{\varepsilon}_{2p}$ in Eq. 3 in the main text, respectively). **(C)** The reduced plasma frequency $\omega_p' = \omega_p/\sqrt{\varepsilon_\infty}$ as a function delay after excitation. **(D)** The volume fraction f of the material with response $\tilde{\varepsilon}_a$.

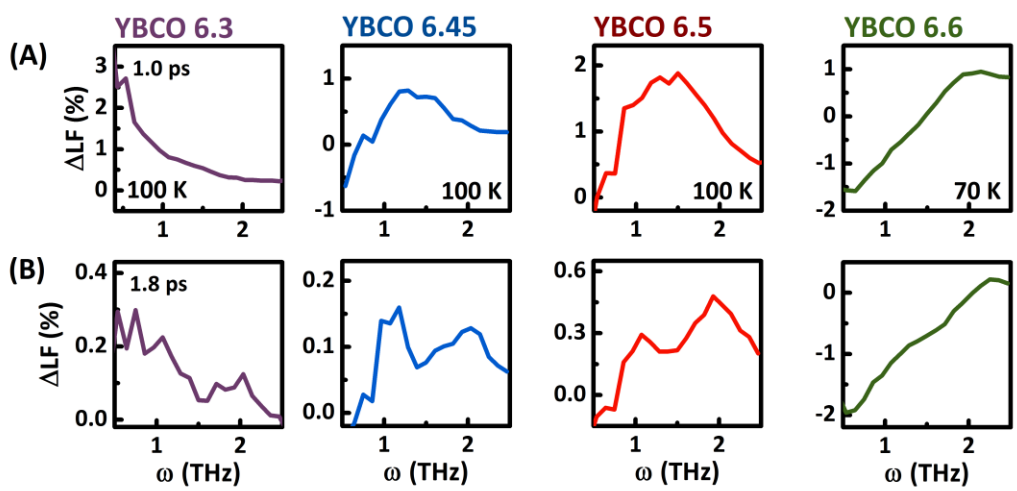

Figure S6.2: Splitting of the light-induced plasma mode. The transient loss function is shown at two time delays, 1.0 ps (top row) and 1.8 ps (bottom row). At early times, a single peak sits at the plasma mode frequency. At later times, the peak splits, indicating two modes.

---

[1] M. Born and E. Wolf, *Principles of Optics*. (Cambridge University Press, Cambridge, 1999) 7th Edition, p. 54-64.

[2] S. Kaiser, C. R. Hunt, D. Nicoletti, W. Hu, I. Gierz, H. Y. Liu, M. Le Tacon, T. Loew, D. Haug, B. Keimer, and A. Cavalleri, "Optically induced coherent transport far above T_c in underdoped $YBa_2Cu_3O_{6+\delta}$," *Phys. Rev. B* **89**, 184516 (2014).

[3] C. R. Hunt, Ph.D. thesis, University of Illinois at Urbana-Champaign, 2015.

[4] C. C. Homes, T. Timusk, D. A. Bonn, R. Liang, and W. N. Hardy. "Optical properties along the c-axis of $YBa_2Cu_3O_{6+x}$ for $x = 0.50 \rightarrow 0.95$ Evolution of the pseudogap" *Physica C* **254**, 265-280 (1995).

[5] T. Timusk, C. C. Homes. "The role of magnetism in forming the *c*-axis spectral peak at 400 cm^{-1} in high temperature superconductors," *Sol. State Comm*. **126**, 63-69 (2003).

[6] C. C. Homes, T. Timusk, D. A. Bonn, R. Liang, and W. N. Hardy. "Optical phonons polarized along the c-axis of $YBa_2Cu_3O_{6+x}$ for $x = 0.50 \rightarrow 0.95$," *Can. J. Phys.* **73**, 663-675 (1995).

[7] C. C. Homes, S. V. Dordevic, D. A. Bonn, R. Liang, W. N. Hardy, and T. Timusk. "Coherence, incoherence, and scaling along the c axis of $YBa_2Cu_3O_{6+x}$," *Phys. Rev. B* **71**, 184515 (2005).

[8] D. Fausti, R. I. Tobey, N. Dean, S. Kaiser, *et al.*, "Light-induced superconductivity in a stripe-ordered cuprate," *Science* **331**, 189 (2011); C. R. Hunt, D. Nicoletti, S. Kaiser, T. Takayama, H. Takagi, and A. Cavalleri, "Two distinct kinetic regimes for the relaxation of light-induced superconductivity in $La_{1.625}Eu_{0.2}Sr_{0.125}CuO_4$," *Phys. Rev. B* **91**, 020505(R) (2015); M. Först, R. I. Tobey, H. Bromberger, S. B. Wilkins, *et al.*, "Melting of charge stripes in vibrationally driven $La_{1.875}Ba_{0.125}CuO_4$: Assessing the respective roles of electronic and lattice order in frustrated superconductors," *Phys. Rev. Lett.* **112**, 157002 (2014).